Cell Reports
Physical Science

CellPress

Article

Ultrastable Mesoporous Hydrogen-Bonded Organic Framework-Based Fiber Composites toward Mustard Gas Detoxification

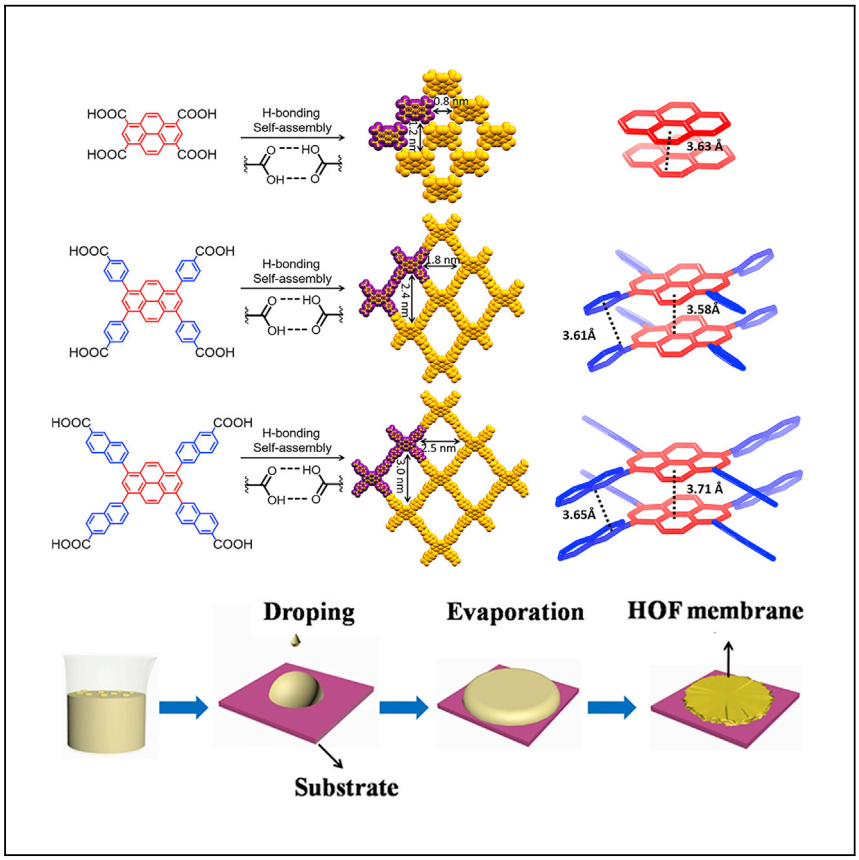

Ma et al. report a "shape-matching" stacking strategy to design and synthesize ultrastable mesoporous hydrogen-bonded organic frameworks (HOFs). The resulting HOF is stable in harsh conditions such as PBS buffer solution and concentrated acids/bases and is easily fabricated into fiber composites for the photochemical detoxification of a mustard gas simulant.

Kaikai Ma, Peng Li, John H. Xin, ..., Rodrigo R. Maldonado, Randall Q. Snurr, Omar K. Farha

penglichem@fudan.edu.cn (P.L.)
o-farha@northwestern.edu (O.K.F.)

HIGHLIGHTS

Ultrastable mesoporous hydrogen-bonded organic frameworks are designed and synthesized

The "shape-matching" stacking avoids staggered stacking and expands pore size to 3 nm

The "shape-matching" stacking enhances thermal and chemical stability of HOF materials

HOF-102 is fabricated into fiber composite for a mustard gas simulant detoxification

Ma et al., Cell Reports Physical Science 1, 100024
February 26, 2020
https://doi.org/10.1016/j.xcrp.2020.100024

Cell Reports
Physical Science

CellPress

Article

Ultrastable Mesoporous Hydrogen-Bonded Organic Framework-Based Fiber Composites toward Mustard Gas Detoxification

Kaikai Ma,[1,2,4,5] Peng Li,[3,5,*] John H. Xin,[4] Yongwei Chen,[1] Zhijie Chen,[1] Subhadip Goswami,[1] Xiaofeng Liu,[1] Satoshi Kato,[1] Haoyuan Chen,[2] Xuan Zhang,[1] Jiaquan Bai,[3] Megan C. Wasson,[1] Rodrigo R. Maldonado,[1] Randall Q. Snurr,[2] and Omar K. Farha[1,6,*]

SUMMARY

Creating crystalline porous materials with large pores is typically challenging due to undesired interpenetration, staggered stacking, or weakened framework stability. Here, we report a pore size expansion strategy by "shape-matching" intermolecular π-π stacking interactions in a series of two-dimensional (2D) hydrogen-bonded organic frameworks (HOFs), HOF-10x (x = 0,1,2), self-assembled from pyrene-based tectons with systematic elongation of π-conjugated molecular arms. This strategy successfully avoids interpenetration or staggered stacking and expands the pore size of HOF materials to access mesoporous HOF-102, which features a surface area of ~2,500 m^2/g and the largest pore volume (1.3 cm^3/g) to date among all reported HOFs. More importantly, HOF-102 shows significantly enhanced thermal and chemical stability as evidenced by powder X-ray diffraction and N_2 isotherms after treatments in challenging conditions. Such stability enables the easy fabrication of a HOF-102/fiber composite for the efficient photochemical detoxification of a mustard gas simulant.

INTRODUCTION

Recently, hydrogen-bonded organic frameworks (HOFs),[1–4] self-assembled from pre-designed molecular tectons using intermolecular H-bonding interactions, are rapidly expanding into a library of novel functional crystalline porous materials with diverse structures and applications including gas storage and separation,[5,6] chiral separation,[7] chemical sensing,[8] proton conduction,[9] and catalysis.[10,11] However, since the first report of HOF materials with permanent microporosity about a decade ago,[12] the development of HOFs has been hindered due to poor stability as a result of the weak H-bonding nature. Alternatively, various synthetic porous solids such as silicates,[13] carbons,[14] metal-organic frameworks (MOFs),[15] and covalent-organic frameworks (COFs)[16] have achieved a wide range of pore sizes from micro- to mesopores. Thus, the augmentation of pore size within HOFs to also access a stable HOF with permanent mesoporosity remains a long-standing challenge.

The isoreticular expansion strategy has been impactful for the construction of MOFs[17–19] and COFs[20,21] with large pores and high surface areas. However, direct extension of ligands to prepare mesoporous HOFs with three-dimensional (3D) structures has typically resulted in a high degree of framework interpenetration,[22–24] significantly reducing the open aperture size and limiting the inclusion of large guest molecules. Besides, large pore size and high stability are usually contradictory to each other and rarely combined into one single porous material.[25,26] Thus,

[1]Department of Chemistry, International Institute of Nanotechnology, Northwestern University, 2145 Sheridan Road, Evanston, IL 60208, USA

[2]Department of Chemical and Biological Engineering, Northwestern University, 2145 Sheridan Road, Evanston, IL 60208, USA

[3]Shanghai Key Laboratory of Molecular Catalysis and Innovative Materials, Department of Chemistry, Fudan University, 2005 Songhu Road, Shanghai 200438, China

[4]Research Centre for Smart Wearable Technology, Institute of Textiles and Clothing, The Hong Kong Polytechnic University, Hong Kong SAR 999077, China

[5]These authors contributed equally

[6]Lead Contact

*Correspondence: penglichem@fudan.edu.cn (P.L.), o-farha@northwestern.edu (O.K.F.)

https://doi.org/10.1016/j.xcrp.2020.100024

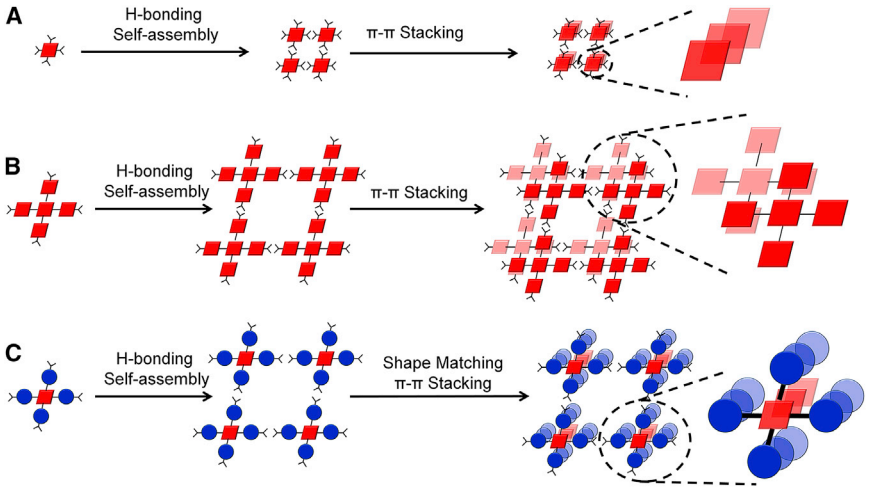

Scheme 1. Schematic Illustration of H-Bonding Self-Assembly and π-π Stacking of Tectons

(A–C) Tecton with (A) one, (B) two same, and (C) two different shapes of fused aromatic rings. Red square and blue circle represent two kinds of fused aromatic rings with different shape. The shape-matching π-π stacking between the fused aromatic rings is shown as a stacking of red square to red square and blue circle to blue circle.

development of an alternative pore size expansion strategy for the construction of stable mesoporous HOF materials is highly desirable. Among various approaches to stabilize HOFs, design of two-dimensional (2D) HOFs with intermolecular π-π interactions was found to be the most effective.[1] π–π stacking interactions are ubiquitous in both Nature, driving nucleobase stacking within DNA and RNA molecules, and in synthetic materials, prompting molecular recognition between various aromatics.[27] Though π-π stacking interactions are not desirable for high surface areas,[28] co-planar π-conjugated large aromatic tectons are ideal for stable HOFs due to their inert reactivity and high chemical resistance to solvent, acid, and base. Such tectons usually form 2D layers by H-bonding, while cooperative π-π stacking interactions exist between 2D layers, which has proved to be a reliable approach to stabilize HOF materials.[8,11,29–32] For example, a series of HOFs with isostructural or quasi-isostructural honeycomb frameworks has been prepared by assembling tectons with C_3- or C_6- symmetries.[29,33] However, as the length of tectons increases, the π-π stacking between 2D layers tends to be in a staggered manner rather than eclipsed, which leads to a decrease in the pore size of these HOFs. In contrast to the eclipsed stacking in H-bonding self-assembly of tectons with one kind of fuse aromatic ring, the staggered stacking is typically observed when tectons with two or more same type of aromatic rings is used (Scheme 1A and 1B).

To address this challenge, we propose to design tectons with two different kinds of connected bulky fused aromatic rings. First, different shape of bulky fused aromatic rings favor to form shape-matching π-π stacking, thus efficiently preventing staggered stacking (Scheme 1C). Second, this strategy can increase the pore size and π-π stacking interactions areas between 2D layers simultaneously, which we hoped would lead to very stable HOF materials. To test our hypothesis, we designed and synthesized a series of HOFs, **HOF-10x** (x = 0,1,2), using tecton molecules based on a pyrene core connected by four molecular arms terminated with carboxylate groups. All three tectons form 2D H-bonded layer structures, which are further stabilized by the eclipsed π-π stacking between layers. More importantly, a systematic investigation of the crystal structure, permanent porosity, and chemical/thermal

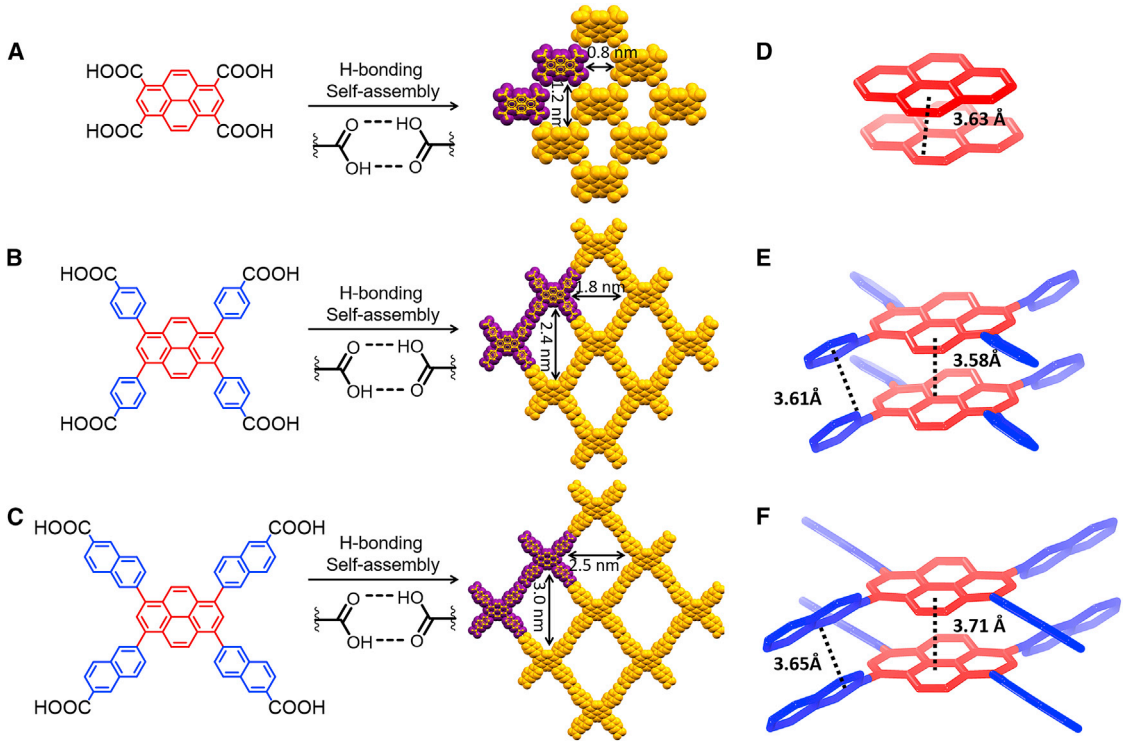

Figure 1. Chemical Structures of Tectons and Crystal Structures of HOFs

(A–C) H-bonding drives the self-assembly of tectons into 2D layers in HOF-100 (A), HOF-101 (B), and HOF-102 (C).

(D–F) "Shape-matching" π-π interactions between 2D layers in HOF-100 (D), HOF-101 (E), and HOF-102 (F).

stability of three isostructural pyrene-based HOFs indicates that the expansion of tectons with shape-matching large fused aromatic rings demonstrates to be an efficient pore expansion strategy without sacrificing the framework stability.

RESULTS

Synthesis and Characterization of Isostructural HOFs

Pyrene, a classic fused benzene ring molecule with planar conformation and large π-conjugated system, is chosen as the center of the tectons. Previously, 1,3,6,8-tetrakis (p-benzoic acid) pyrene (H_4TBAPy) has been used to construct a stable HOF, known as PFC-1[11] (we name it as **HOF-101** as this material was made prior to the publication of PFC-1). To systematically study the influence of intermolecular π-π interactions on the stability of HOFs, two additional pyrene-based tectons analogs to H_4TBAPy (Figures 1A–1C), 1,3,6,8-tetracarboxy pyrene (H_4TCPy) (Figures S1 and S2) and 1,3,6,8-tetra(6-carboxynaphthalen-2-yl) pyrene (H_4TNAPy), were synthesized to build an isostructural HOF family. Microcrystals of the HOF materials (**HOF-100**, **HOF-101**, and **HOF-102**) can be easily made via a fast precipitation method by introducing acetone into a concentrated *N*,*N*-dimethylformamide (DMF) solution of corresponding tectons (Figures S3–S5). However, the crystal structures of **HOF-100** and **HOF-102** were not fully solved by single-crystal X-ray diffraction measurements, and only their unit cells were determined. With the experimental unit cell and a molecular modeling method, we simulated the crystal structure of **HOF-100** and **HOF-102** from powder X-ray diffractions (PXRD) (Table S1; Figures S6 and S7). As expected, the resulting HOFs featured a H-bonding self-assembled 2D layer structure through carboxy dimer complementary H-bonds. See Figure 1. Each layer stacks with the neighboring one as AA mode along the (100) direction to form one-dimensional

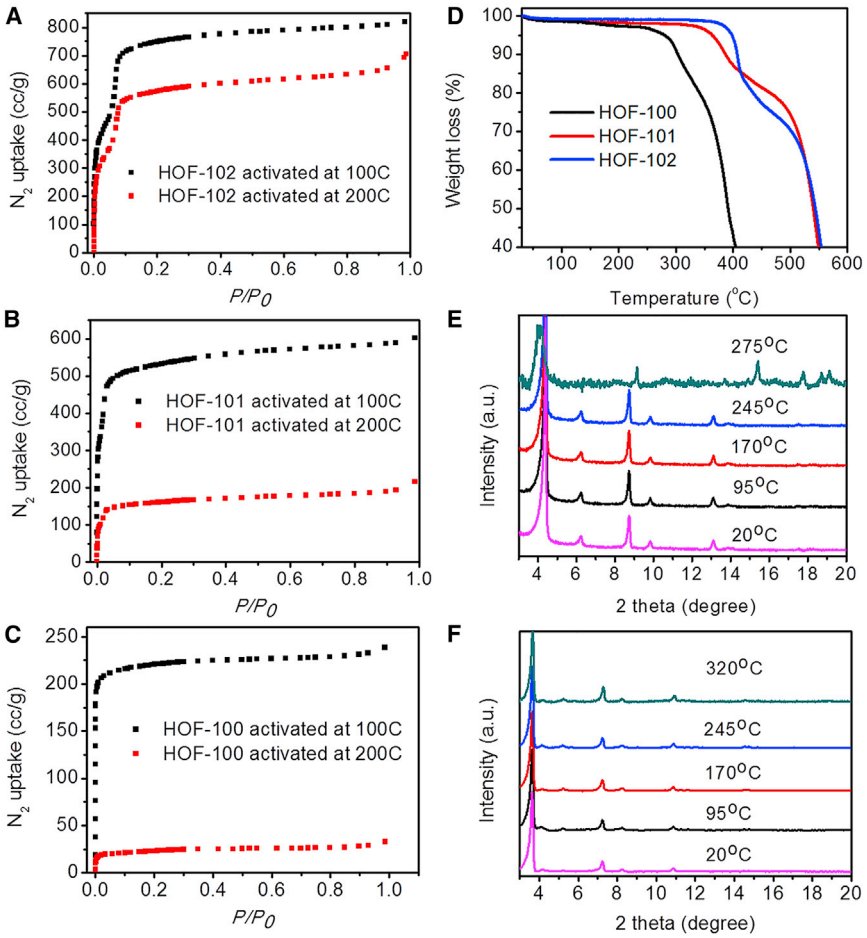

Figure 2. Thermal Stability Tests of HOFs

(A–C) N_2 isotherms at 77 K of HOF-102 (A), HOF-101 (B), and HOF-100 (C) activated at different temperature.

(D) TGA curves of HOFs.

(E and F) Variable-temperature PXRD patterns of HOF-101 (E) and HOF-102 (F).

channels. The resulting channels in these HOFs show a systematic increase of pore size (diagonal dimensions: 0.8 × 1.2 nm for **HOF-100**, 1.8 × 2.4 nm for **HOF-101**, and 2.5 × 3.0 nm for **HOF-102**). Further examination of the neighboring layers of these HOFs indicates strong π-π interactions (Figures 1D–1F). The porosity of solvent-free (activated) **HOF-100**, **HOF-101**, and **HOF-102** was determined through N_2 physisorption measurements isotherms collected at 77 K (Figures 2A–2C). The following trend of N_2 uptake capacity was observed: **HOF-100** (235 cm^3/g) < **HOF-101** (605 cm^3/g) < **HOF-102** (815 cm^3/g). Importantly, **HOF-100** and **HOF-101** (a small step of mesopore uptake was observed) showed typical type I isotherms of microporous materials, while **HOF-102** displayed a type IV isotherms, indicative of mesoporous materials. The Brunauer-Emmett-Teller (BET) areas were calculated to be 900 m^2 g for **HOF-100**, 2,100 m^2 g for **HOF-101**, and 2,500 m^2 g for **HOF-102**. Additionally, the pore volume of **HOF-102** (1.3 cm^3/g), to the best of our knowledge, is the highest among HOF materials (Table S2). To accurately determine the pore size distribution of activated **HOF-102**, an Ar physisorption measurement was performed at 87 K and yielded a type IV isotherm as expected. The pore size distribution obtained using a non-local density functional theory (NLDFT) model

Table 1. Chemical Stability against Various Chemical Media

Porous Materials	Water, RT	Boiling Water	PBS Buffer (pH 7.4)	HCl (pH 1)	NaOH (pH 12)	NaOH (pH 14)	HCl (12M)	H_2SO_4 (18M)
HOF-102	√	√	√	√	√	√	√	√
HOF-101	√	√	√	√	×	×	√	√
HOF-100	√	×	√	√	×	×	√	×
HKUST-1	×	×	×	×	×	×	×	×
UiO-66	√	√	×	√	×	×	×	×
ZIF-8	√	√	×	×	√	√	×	×

indicated a mesopore centered at 2.8 nm (Figure S8). To evaluate the π-π interaction energies of these HOFs, we performed DFT calculations with both dispersion and counterpoise corrections on the π-π stacked dimers (details in Supplemental Information). The energy dramatically increased from −53.4 kJ/mol for **HOF-100**, −137 kJ/mol for **HOF-101**(PFC-1), to −208 kJ/mol for **HOF-102** (Table S3). The values for **HOF-101** and **HOF-102** were higher than that of H-bonding energy (−99.4 kJ/mol), demonstrating that structural stability of these HOFs can be attributed in part to the π-π stacking interactions.

Thermal and Chemical Stability Tests

To experimentally support the calculated π-π energies in these HOFs, we probed their thermal and chemical stabilities. First, we tested the thermal stability by activating the HOFs materials under 100°C and 200°C and then compared the N_2 isotherms (Figures 2A–2C). **HOF-102** exhibited only a small decrease (13%) in N_2 uptake at the higher temperature, while the losses in **HOF-101** (67%) and **HOF-100** (84%) were larger. In addition, according to thermogravimetric analysis (TGA) under nitrogen (Figure 2D), the thermal decomposition temperatures of HOFs are in the order: 370°C (**HOF-102**) > 310°C (**HOF-101**) > 250°C (**HOF-100**). *In situ* variable-temperature PXRD showed PXRD peak broadening and shifting for **HOF-101** at 275°C (Figure 2E), while the crystallinity of **HOF-102** remained unchanged up to 320°C (Figure 2F). The TGAs demonstrate that **HOF-102** can be thermally stable up to 420°C, which is significantly higher than that of **HOF-101** (370°C) and **HOF-100** (280°C) (Figure S9). To investigate the chemical stabilities of these HOFs, we exposed **HOF-10x** (x = 0,1,2) to a series of challenging conditions, including different organic solvents (such as tetrahydrofuran, dichloromethane, ethanol, and acetone), water vapor, boiling water, PBS buffer, pH 1/pH 12/pH 14 aqueous solution, concentrated HCl (12M), and H_2SO_4 (18M) solution (Table 1). **HOF-102** maintained its crystallinity after treatment under these conditions, as demonstrated by PXRD (Figure 3A), mass-balance studies (Figure S10), and N_2 isotherms after treatments (Figure 3B). In comparison, the chemical stabilities of **HOF-10x** (x = 0,1,2) are in agreement with the π-π energy calculation trend. **HOF-100** and **HOF-101** both dissolve quickly in NaOH solution (pH 12) solution, and **HOF-100** loses its crystallinity in the presence of boiling water and concentrated H_2SO_4 (Figures S11 and S12). To further compare the chemical stabilities of these HOFs with other porous materials, several highly robust, benchmark MOFs (HKUST-1[34], UiO-66,[35] and ZIF-8[36]) were also tested (Figures S13–S16). The MOFs did not retain their crystallinity under certain conditions (Table 1; Figures S17-S19), most notably under PBS buffer, strong inorganic acid, and pH 14 basic solution.

The surface wettability of the HOFs was characterized using contact-angle measurements (Figure S20). The contact angles of water and decane on **HOF-10x** (x = 0,1,2)

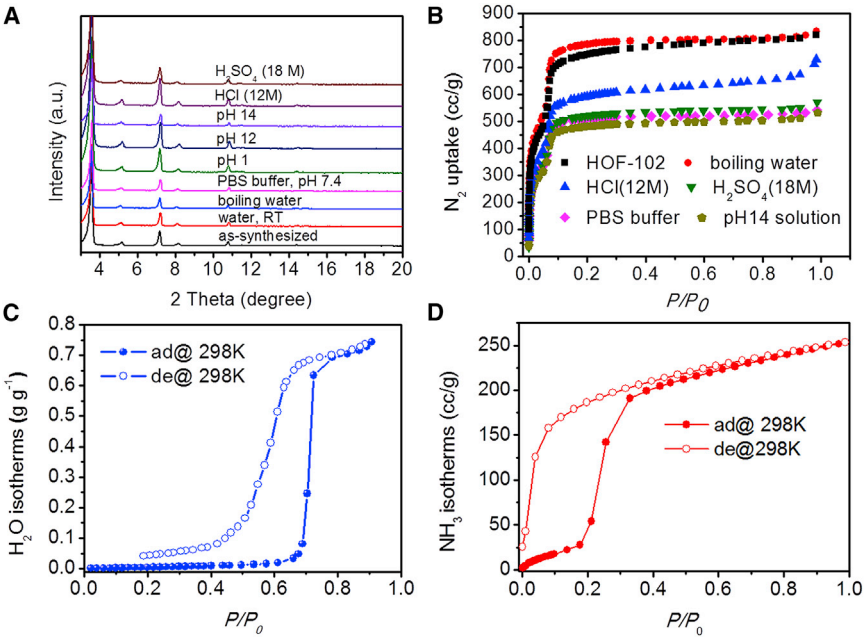

Figure 3. Chemical Stability Tests and H_2O/NH_3 Isotherms of HOF-102

(A and D) PXRD patterns (A) and N_2 isotherms (B) at 77 K of HOF-102 after treatments in various challenging conditions.

(C and D) Water vapor (C) and NH_3 isotherms (D) of HOF-102 at 298 K.

were between 8° and 15°, indicating the amphiphilic nature of these materials. The exceptional stability of **HOF-102** prompted us to explore the adsorption performance of water vapor and ammonia. The water vapor and ammonia isotherms of **HOF-102** were measured at 298 K (Figures 3C and 3D). The PXRD measurements suggest that **HOF-102** is still crystalline in the presence of water vapor and NH_3 (Figure S21). Therefore, the ultra-high chemical stability of **HOF-102** against harsh aqueous conditions was not due to its hydrophobicity and can be attributed to the high π-π stacking interactions. The water vapor loading capacity of **HOF-102** at 1 atm is 0.7 g/g, and the ammonia uptake capacity is about 250 cm^3/g at 1 atm, which are comparable with the water vapor and NH_3 sorption abilities of MOF materials.[37–39]

Adsorption of Dyes and Biomolecule in Water

To take advantage of this chemical stability, we explored the potential of **HOF-102** as a sorbent in water media and tested its ability to adsorb a cationic dye methylene blue (MB) and an anionic dye resorufin sodium salt (RS). The uptake kinetics were measured at a 200 ppm initial concentration by measuring the change of UV-vis spectra at given time intervals (Figures S22 and S23). Remarkably, both cationic MB and anionic RS were absorbed by **HOF-102** quickly from the aqueous solution within a few minutes. The adsorbed MB or RS was washed away by organic solvent such that **HOF-102** was reused for at least 6 times without losing its adsorption capabilities (Figures 4A–4D). The slightly faster adsorption of MB than RS by **HOF-102** was attributed to the likely coulombic affinity between negatively charged deprotonated carboxylate in **HOF-102** and MB. To understand the adsorption of MB on **HOF-102**, isothermal titration calorimetry (ITC) experiments (Figure S24; Table S4) were performed, and the calculated binding affinity (K_a = 3.89 ± 0.22 × 10^4 M^{-1}) for MB on **HOF-102** is higher than the reported value using carbon nanotube as a sorbent.[40] Encouraged by the sorption performance of **HOF-102** in water,

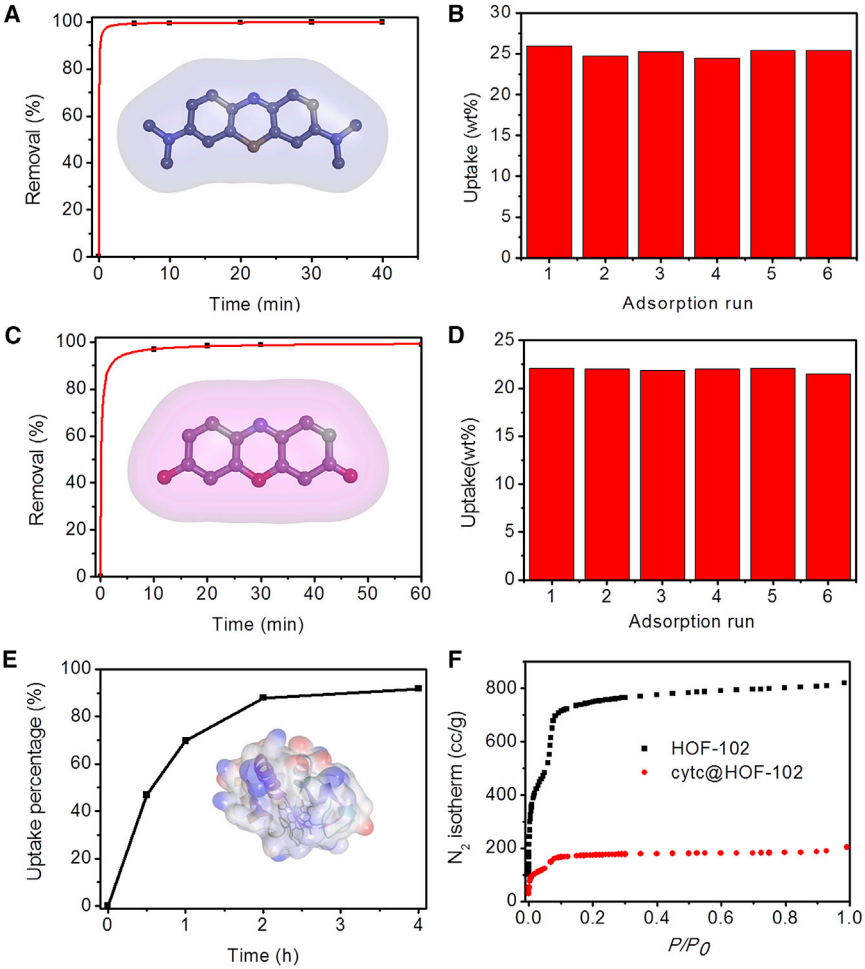

Figure 4. Adsorption Dyes and Biomolecule in Water Using HOF-102

(A–D) Adsorption kinetics and recyclabilities of HOF-102 for methylene blue (MB; A and B) and resorufin sodium salt (RS; C and D).

(E) Adsorption of cytochrome *c* by HOF-102.

(F) N_2 isotherms at 77K of HOF-102 before and after cytochrome *c* uptake.

cytochrome *c* (Cyt-c, 3.6 × 2.4 × 2.2 nm)[41] was selected to probe the capability of **HOF-102** as an adsorbent for macromolecules. It was expected that Cyt-c could access the pores of **HOF-102** because of the similar dimensions of the square aperture of **HOF-102** (2.4 nm) with the short dimensions of Cyt-c. Activated **HOF-102** was soaked in a buffer solution of Cyt-c, and the macromolecule's concentration was monitored by UV-vis spectroscopy in solution (Figure S25). The complete adsorption of Cyt-c occurred within 4 h (Figure 4E). The color of **HOF-102** turned from yellow to orange to form a Cyt-c@**HOF-102** composite, and the sorption capacity was ~30 w %. Retained crystallinity was observed in the PXRD of Cyt-c@**HOF-102** (Figure S26). N_2 isotherms (Figure 4F) and pore size distributions (Figure S27) indicated the occupation of Cyt-c within the mesopores of **HOF-102** due to a significant decrease of pore volume.

Fabrication of HOF/Fiber Composites for Photocatalysis

Inspired by the observed high stability of **HOF-102**, we set out to fabricate **HOF-102** on fibers to form flexible and wearable materials. An acetone suspension of

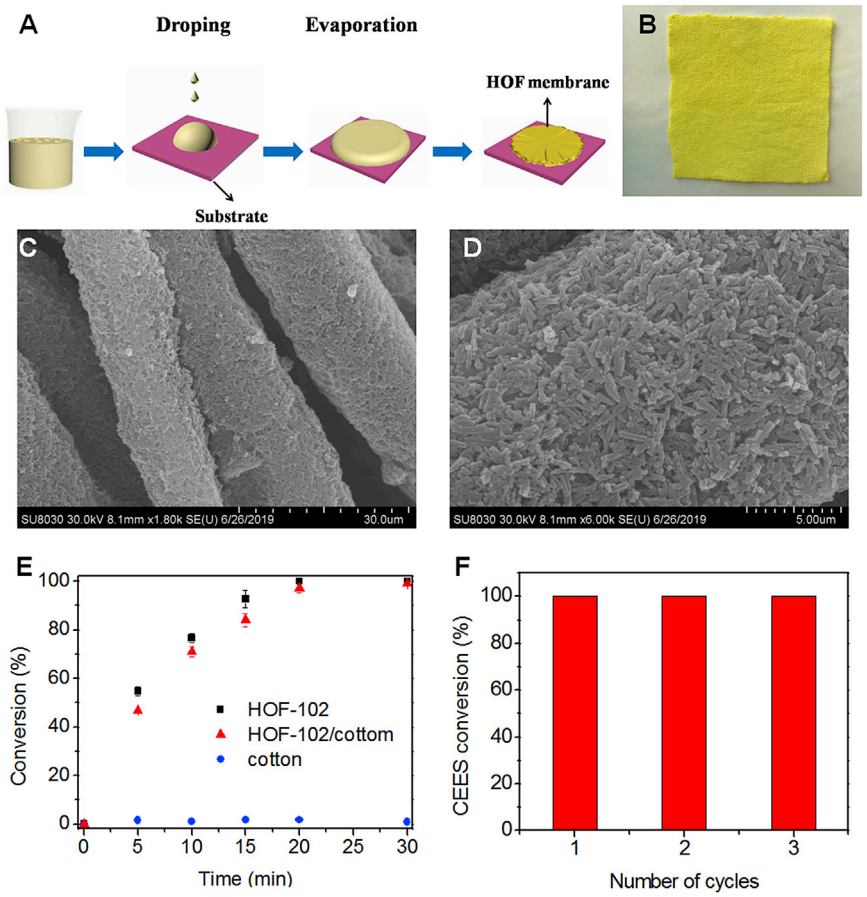

Figure 5. Preparation and Photochemical Catalysis of HOF/Fiber Composite

(A) Dropcasting method for HOF/fiber preparation.

(B–D) Photograph (B) and SEM images (C and D) of HOF/fiber composite.

(E and F) Kinetic study (E; error bar: n = 3, $p < 0.05$) and catalyst reusability (F) for the photooxidation of the mustard gas simulant CEES by HOF-102 alone and HOF-102/fiber composite.

HOF-102 nanocrystals was dropcast onto a cotton fiber surface followed by solvent evaporation at ambient conditions (Figures 5A and 5B). The uniform **HOF-102** coating on fiber was observed through scanning electron microscopy (SEM) images (Figures 5C and 5D). The crystallinity and porosity of the HOF/fiber composite were examined by PXRD and N_2 isotherms (Figures S28 and S29), which were in good agreement to the free powder samples of **HOF-102**. Previously, our group has demonstrated that the H_4TBAPy-based MOF NU-1000[42] can be used as a stable photocatalyst for the selective aerobic oxidation of the mustard gas simulant, 2-chloroethyl ethyl sulfide (CEES) to the nontoxic product 2-chloroethyl ethyl sulfoxide (CEESO) by LED (light-emitting diode) irradiation of appropriate wavelength. As a proof of concept for the utility of the composite, we investigated the performance of **HOF-102**/fiber as a composite photocatalyst by utilizing the pyrene-based chromophores in the HOF structure. With 1 mol% catalyst used (based on pyrene), the HOF-102/fiber composite converted 48% of the starting material in 5 min and 100% in 30 min (Figure 5E), as monitored through gas chromatography-mass spectrometry (GC-MS). The activity of **HOF-102/cotton** is close to the pure **HOF-102** and there is negligible activity for cotton. The selectivity of the catalytic reaction for the mono-oxygenated product (CEESO) over the overoxidized toxic 2-chloroethyl ethyl sulfone ($CEESO_2$) was confirmed via ^{1}H nuclear magnetic resonance (NMR)

spectroscopy of the reaction mixture (Figures S30 and S31). Furthermore, it was reused for at least three times without compromising catalytic activity (Figure 5F) due to bleaching of the chromophore, and the maintained crystallinity in the PXRD of **HOF-102** after catalysis demonstrated the material's chemical stability under the reaction conditions. Considering the flexibility and high mechanical stability of fiber materials, HOF/fiber composite materials has the potential to be used as mustard gas protective gear in the future.

DISCUSSION

A pore-expansion strategy based on "shape-matching" intermolecular π-π stacking interactions was developed to prepare a series of isostructural HOF materials, **HOF-10x** (x = 0,1,2), with tunable pore size and enhanced stabilities. The mesoporous **HOF-102** was stable in harsh conditions such as PBS buffer solution and concentrated acids/bases, indicating viability as an efficient and durable adsorbent material for Cyt c in aqueous solution. The developed strategy to access high stability in **HOF-102** also demonstrated solution processability with the deposition of the material on fiber to obtain a photochemically active composite material. We are hopeful that this work will open an avenue for the rational design and synthesis of additional mesoporous HOF materials with impressive stabilities and solution processabilities.

EXPERIMENTAL PROCEDURES

General Procedure for HOF Synthesis

HOF-10x (x = 0,1,2) was synthesized by introducing acetone into linker solution in DMF. With **HOF-102** as an example, H_4TNAPy (200 mg, 0.225 mmol) was dissolved in 60 mL of DMF under heating at 120°C for 1 h to get a clear yellow solution. After cooling down to room temperature, H_4TNAPy solution was poured into 160 mL of acetone under stirring (400 rpm) within 2 min. The suspension was kept stirring for 12 h and isolated by centrifugation at 8,000 rpm for 5 min. The obtained yellow powder was further washed with acetone (4 × 45 mL) and then dried in at room temperature (yield 178 mg, 89%). See Supplemental Experimental Procedures for further details.

General Procedure for Chemical Stability Test

50 mg of HOFs or MOFs powder was immersed into 30 mL of HCl (12 M), H_2SO_4 (18M), water (pH 1, 12, and 14), PBS (pH 7.2), and boiling water for 24 h. The samples were then isolated by centrifugation and washed by water (3 × 45 mL) and acetone (3 × 45 mL). Then, they were dried under vacuum at 80°C for 12 h before the PXRD or N_2 adsorption test.

General Procedures for Fabrication of HOF/Fiber Composite

70 mg **HOF-102** was dispersed into 2 mL of acetone under ultrasonication for 2 min to get a uniform suspension. The 1 mL of suspension was drop casted onto cotton textile (400 mg, 5 cm × 5 cm) carefully, and the textile was dried in a hood overnight to evaporate the solvent, and then the drop casting procedure was repeated again on the dried textile piece to get a mass loading about 15% on fiber.

DATA AND CODE AVAILABILITY

The authors declare that data supporting the findings of this study are available within the paper and the Supplemental Information. All other data are available from the lead contact upon reasonable request.

SUPPLEMENTAL INFORMATION

Supplemental Information can be found online at https://doi.org/10.1016/j.xcrp.2020.100024.

ACKNOWLEDGMENTS

O.K.F. gratefully acknowledges DTRA for financial support (HDTRA1-19-1-0010) and Northwestern University for their continued support of this research. P L. would like to thank the start-up funding from Fudan University. R.Q.S. thanks DTRA for financial support under HDTRA1-18-1-0003.

AUTHOR CONTRIBUTIONS

O.K.F. and P.L. planned and directed the project. K.M., Y.C., and R.R.M. synthesized the HOFs and collected and analyzed the gas adsorption, X-ray diffraction, SEM, and stability tests under the supervision of O.K.F and P.L.; K.M. prepared the HOF/fiber composite under the guidance of J.H.X.; J.B. and X.L. prepared the tectons of HOFs under the supervision of P.L.; S.G. measured the photocatalysis of HOF/fiber composite; Z.C. obtained the H_2O and NH_3 isotherms; X.Z. performed phase analysis and Pawley refinement on the simulated HOF structures. H.C. calculated the π-π interaction energies under the supervision of R.S.; S.K. measured the ITC experiments; K.M., M.C.W., and P.L. wrote the initial paper draft, and all authors contributed to revising the paper.

DECLARATION OF INTERESTS

The authors declare no competing interests.

Received: August 22, 2019
Revised: November 17, 2019
Accepted: January 13, 2020
Published: February 12, 2020

REFERENCES

1. Lin, R.-B., He, Y., Li, P., Wang, H., Zhou, W., and Chen, B. (2019). Multifunctional porous hydrogen-bonded organic framework materials. Chem. Soc. Rev. *48*, 1362–1389.

2. Hisaki, I., Xin, C., Takahashi, K., and Nakamura, T. (2019). Designing Hydrogen-Bonded Organic Frameworks (HOFs) with Permanent Porosity. Angew. Chem. Int. Ed. Engl. *58*, 11160–11170.

3. Luo, J., Wang, J.-W., Zhang, J.-H., Lai, S., and Zhong, D.-C. (2018). Hydrogen-bonded organic frameworks: design, structures and potential applications. CrystEngComm *20*, 5884–5898.

4. Hasell, T., and Cooper, A.I. (2016). Porous organic cages: soluble, modular and molecular pores. Nat. Rev. Mater. *1*, 16053.

5. Lü, J., and Cao, R. (2016). Porous organic molecular frameworks with extrinsic porosity: A platform for carbon storage and separation. Angew. Chem. Int. Ed. Engl. *55*, 9474–9480.

6. Pulido, A., Chen, L., Kaczorowski, T., Holden, D., Little, M.A., Chong, S.Y., Slater, B.J., McMahon, D.P., Bonillo, B., Stackhouse, C.J., et al. (2017). Functional materials discovery using energy-structure-function maps. Nature *543*, 657–664.

7. Li, P., He, Y., Guang, J., Weng, L., Zhao, J.C.-G., Xiang, S., and Chen, B. (2014). A homochiral microporous hydrogen-bonded organic framework for highly enantioselective separation of secondary alcohols. J. Am. Chem. Soc. *136*, 547–549.

8. Hisaki, I., Suzuki, Y., Gomez, E., Ji, Q., Tohnai, N., Nakamura, T., and Douhal, A. (2019). Acid Responsive Hydrogen-Bonded Organic Frameworks. J. Am. Chem. Soc. *141*, 2111–2121.

9. Karmakar, A., Illathvalappil, R., Anothumakkool, B., Sen, A., Samanta, P., Desai, A.V., Kurungot, S., and Ghosh, S.K. (2016). Hydrogen-Bonded Organic Frameworks (HOFs): A New Class of Porous Crystalline Proton-Conducting Materials. Angew. Chem. Int. Ed. Engl. *55*, 10667–10671.

10. Han, B., Wang, H., Wang, C., Wu, H., Zhou, W., Chen, B., and Jiang, J. (2019). Postsynthetic Metalation of a Robust Hydrogen-Bonded Organic Framework for Heterogeneous Catalysis. J. Am. Chem. Soc. *141*, 8737–8740.

11. Yin, Q., Zhao, P., Sa, R.J., Chen, G.C., Lü, J., Liu, T.F., and Cao, R. (2018). An Ultra-Robust and Crystalline Redeemable Hydrogen-Bonded Organic Framework for Synergistic Chemo-Photodynamic Therapy. Angew. Chem. Int. Ed. Engl. *57*, 7691–7696.

12. He, Y., Xiang, S., and Chen, B. (2011). A microporous hydrogen-bonded organic framework for highly selective C_2H_2/C_2H_4 separation at ambient temperature. J. Am. Chem. Soc. *133*, 14570–14573.

13. Liebau, F. (2012). Structural Chemistry of Silicates: Structure, Bonding, and Classification (Springer Science & Business Media).

14. Ryoo, R., Joo, S.H., Kruk, M., and Jaroniec, M. (2001). Ordered mesoporous carbons. Adv. Mater. *13*, 677–681.

15. Furukawa, H., Cordova, K.E., O'Keeffe, M., and Yaghi, O.M. (2013). The chemistry and applications of metal-organic frameworks. Science *341*, 1230444.

16. Yaghi, O.M., Kalmutzki, M.J., and Diercks, C.S. (2019). Introduction to Reticular Chemistry: Metal-Organic Frameworks and Covalent Organic Frameworks (Wiley).

17. Li, P., Chen, Q., Wang, T.C., Vermeulen, N.A., Mehdi, B.L., Dohnalkova, A., Browning, N.D., Shen, D., Anderson, R., Gómez-Gualdrón, D.A., et al. (2018). Hierarchically engineered mesoporous metal–organic frameworks toward cell-free immobilized enzyme systems. Chem *4*, 1022–1034.

18. Farha, O.K., Yazaydın, A.Ö., Eryazici, I., Malliakas, C.D., Hauser, B.G., Kanatzidis, M.G., Nguyen, S.T., Snurr, R.Q., and Hupp, J.T. (2010). De novo synthesis of a metal-organic framework material featuring ultrahigh surface area and gas storage capacities. Nat. Chem. *2*, 944–948.

19. Deng, H., Grunder, S., Cordova, K.E., Valente, C., Furukawa, H., Hmadeh, M., Gándara, F., Whalley, A.C., Liu, Z., Asahina, S., et al. (2012). Large-pore apertures in a series of metal-organic frameworks. Science *336*, 1018–1023.

20. Biswal, B.P., Chandra, S., Kandambeth, S., Lukose, B., Heine, T., and Banerjee, R. (2013). Mechanochemical synthesis of chemically stable isoreticular covalent organic frameworks. J. Am. Chem. Soc. *135*, 5328–5331.

21. Guan, X., Li, H., Ma, Y., Xue, M., Fang, Q., Yan, Y., Valtchev, V., and Qiu, S. (2019). Chemically stable polyarylether-based covalent organic frameworks. Nat. Chem. *11*, 587–594.

22. Li, P., Li, P., Ryder, M.R., Liu, Z., Stern, C.L., Farha, O.K., and Stoddart, J.F. (2019). Interpenetration Isomerism in Triptycene-Based Hydrogen-Bonded Organic Frameworks. Angew. Chem. Int. Ed. Engl. *58*, 1664–1669.

23. Lü, J., Perez-Krap, C., Suyetin, M., Alsmail, N.H., Yan, Y., Yang, S., Lewis, W., Bichoutskaia, E., Tang, C.C., Blake, A.J., et al. (2014). A robust binary supramolecular organic framework (SOF) with high CO2 adsorption and selectivity. J. Am. Chem. Soc. *136*, 12828–12831.

24. Boer, S.A., Morshedi, M., Tarzia, A., Doonan, C.J., and White, N.G. (2019). Molecular Tectonics: A Node-and-Linker Building Block Approach to a Family of Hydrogen-Bonded Frameworks. Chemistry *25*, 10006–10012.

25. Cai, G., and Jiang, H.L. (2017). A Modulator-Induced Defect-Formation Strategy to Hierarchically Porous Metal-Organic Frameworks with High Stability. Angew. Chem. Int. Ed. Engl. *56*, 563–567.

26. Huang, H., Li, J.-R., Wang, K., Han, T., Tong, M., Li, L., Xie, Y., Yang, Q., Liu, D., and Zhong, C. (2015). An in situ self-assembly template strategy for the preparation of hierarchical-pore metal-organic frameworks. Nat. Commun. *6*, 8847.

27. Rossow, T., and Seiffert, S. (2015). Supramolecular polymer networks: Preparation, properties, and potential. In Supramolecular Polymer Networks and Gels, S. Seiffert, ed. (Springer), pp. 1–46.

28. Mastalerz, M., and Oppel, I.M. (2012). Rational construction of an extrinsic porous molecular crystal with an extraordinary high specific surface area. Angew. Chem. Int. Ed. Engl. *51*, 5252–5255.

29. Hisaki, I., Ikenaka, N., Gomez, E., Cohen, B., Tohnai, N., and Douhal, A. (2017). Hexaazatriphenylene-Based Hydrogen-Bonded Organic Framework with Permanent Porosity and Single-Crystallinity. Chemistry *23*, 11611–11619.

30. Hisaki, I., Suzuki, Y., Gomez, E., Cohen, B., Tohnai, N., and Douhal, A. (2018). Docking Strategy To Construct Thermostable, Single-Crystalline, Hydrogen-Bonded Organic Framework with High Surface Area. Angew. Chem. Int. Ed. Engl. *57*, 12650–12655.

31. Chen, T.-H., Popov, I., Kaveevivitchai, W., Chuang, Y.-C., Chen, Y.-S., Daugulis, O., Jacobson, A.J., and Miljanić, O.S. (2014). Thermally robust and porous noncovalent organic framework with high affinity for fluorocarbons and CFCs. Nat. Commun. *5*, 5131.

32. Hashim, M.I., Le, H.T.M., Chen, T.-H., Chen, Y.-S., Daugulis, O., Hsu, C.-W., Jacobson, A.J., Kaveevivitchai, W., Liang, X., Makarenko, T., et al. (2018). Dissecting Porosity in Molecular Crystals: Influence of Geometry, Hydrogen Bonding, and [$\pi\cdots\pi$] Stacking on the Solid-State Packing of Fluorinated Aromatics. J. Am. Chem. Soc. *140*, 6014–6026.

33. Hisaki, I., Nakagawa, S., Ikenaka, N., Imamura, Y., Katouda, M., Tashiro, M., Tsuchida, H., Ogoshi, T., Sato, H., Tohnai, N., and Miyata, M. (2016). A series of layered assemblies of hydrogen-bonded, hexagonal networks of C_3-symmetric π-conjugated molecules: A potential motif of porous organic materials. J. Am. Chem. Soc. *138*, 6617–6628.

34. McHugh, L.N., McPherson, M.J., McCormick, L.J., Morris, S.A., Wheatley, P.S., Teat, S.J., McKay, D., Dawson, D.M., Sansome, C.E.F., Ashbrook, S.E., et al. (2018). Hydrolytic stability in hemilabile metal-organic frameworks. Nat. Chem. *10*, 1096–1102.

35. Kandiah, M., Nilsen, M.H., Usseglio, S., Jakobsen, S., Olsbye, U., Tilset, M., Larabi, C., Quadrelli, E.A., Bonino, F., and Lillerud, K.P. (2010). Synthesis and stability of tagged UiO-66 Zr-MOFs. Chem. Mater. *22*, 6632–6640.

36. Park, K.S., Ni, Z., Côté, A.P., Choi, J.Y., Huang, R., Uribe-Romo, F.J., Chae, H.K., O'Keeffe, M., and Yaghi, O.M. (2006). Exceptional chemical and thermal stability of zeolitic imidazolate frameworks. Proc. Natl. Acad. Sci. USA *103*, 10186–10191.

37. Morris, W., Doonan, C.J., and Yaghi, O.M. (2011). Postsynthetic modification of a metal-organic framework for stabilization of a hemiaminal and ammonia uptake. Inorg. Chem. *50*, 6853–6855.

38. Rieth, A.J., Tulchinsky, Y., and Dincă, M. (2016). High and Reversible Ammonia Uptake in Mesoporous Azolate Metal-Organic Frameworks with Open Mn, Co, and Ni Sites. J. Am. Chem. Soc. *138*, 9401–9404.

39. Chen, Z., Li, P., Zhang, X., Li, P., Wasson, M.C., Islamoglu, T., Stoddart, J.F., and Farha, O.K. (2019). Reticular Access to Highly Porous acs-MOFs with Rigid Trigonal Prismatic Linkers for Water Sorption. J. Am. Chem. Soc. *141*, 2900–2905.

40. Ortega, P.F., Trigueiro, J.P.C., Santos, M.R., Denadai, A.M., Oliveira, L.C.A., Teixeira, A.P.C., Silva, G.G., and Lavall, R.L. (2017). Thermodynamic study of methylene blue adsorption on carbon nanotubes using isothermal titration calorimetry: a simple and rigorous approach. J. Chem. Eng. Data *62*, 729–737.

41. Li, P., Vermeulen, N.A., Malliakas, C.D., Gómez-Gualdrón, D.A., Howarth, A.J., Mehdi, B.L., Dohnalkova, A., Browning, N.D., O'Keeffe, M., and Farha, O.K. (2017). Bottom-up construction of a superstructure in a porous uranium-organic crystal. Science *356*, 624–627.

42. Howarth, A.J., Buru, C.T., Liu, Y., Ploskonka, A.M., Hartlieb, K.J., McEntee, M., Mahle, J.J., Buchanan, J.H., Durke, E.M., Al-Juaid, S.S., et al. (2017). Postsynthetic incorporation of a singlet oxygen photosensitizer in a metal–organic framework for fast and selective oxidative detoxification of sulfur mustard. Chemistry *23*, 214–218.